Hydrothermal synthesis of sodium potassium niobate solid solutions at 200 °C†

Albertus D. Handoko[a,b] and Gregory K. L. Goh*[a]

Received 13th November 2009, Accepted 13th January 2010
First published as an Advance Article on the web 20th February 2010
DOI: 10.1039/b923840a

For the first time, a series of sodium potassium niobate solid solutions with compositions around the morphotropic phase boundary (MPB) are hydrothermally synthesized at 200 °C using a simple KOH and NaOH mixture with Nb_2O_5 as a precursor powder. Rietveld refinement of X-ray diffraction data indicated the presence of a second sodium niobate perovskite phase when the concentration of NaOH (compared to the total hydroxyl ion concentration) is above 11.7%. The presence of the second phase is attributed to the different solubilities of the intermediate potassium and sodium hexaniobate species. It is also found that heat-treating the mixed-phase powders for two hours at a temperature of 800 °C is effective in obtaining the desired single-phase solid solution with compositions near the MPB, thereby opening the way to using hydrothermal synthesis in simplifying the laborious solid-state process.

Introduction

$Pb(Zr,Ti)O_3$ (PZT) based ceramics are high-performance piezoelectric materials, extensively used in sensors, actuators and other piezoelectric devices. Their properties are best near the morphotropic phase boundary (MPB), a discontinuous change in the crystal structure when the tetragonal unit cell changes to a rhombohedral one as Zr increasingly substitutes the Ti.[1,2] At the MPB composition, lead makes up to 60% of the total PZT weight,[3] therefore posing a serious hazard to the human central nervous system due to its ability to bind strongly to proteins.[4] Since present processes require high-temperature steps in the synthesis of PZT, lead poisoning can occur due to the ease of PbO volatility.[5] Currently, PZT is exempted from the Restriction of the Use of Certain Hazardous Substances regulation[6] (RoHS – a law enacted in the European Union to limit the amount of hazardous elements in a product) because a similarly high performance material has not yet been demonstrated. Therefore, the need to continue the search for a suitable replacement is imperative.

$(Na_xK_{1-x})NbO_3$ (NKN), a sodium-substituted potassium niobate, is a suitable candidate to replace PZT. This is because like PZT, a morphotrophic phase boundary (MPB) exists when the sodium replaces ~50% of the potassium sites,[7,8] causing an abrupt change from an orthorhombic unit cell (*Amm*2, 2 formula units) to a monoclinic one (*P*1*m*1, 8 formula units). In order to compare the lattice parameters across the phase boundary, expressing the lattice parameters in terms of a pseudocubic unit cell (1 formula unit) is useful and widely used in the perovskite systems.[9] These various unit cells are illustrated in Fig. 1. At the MPB, a material is able to accommodate large atomic displacements,[10] which, depending on the symmetry, may allow the polarization alignment that results in a very high electromechanical coupling.[11]

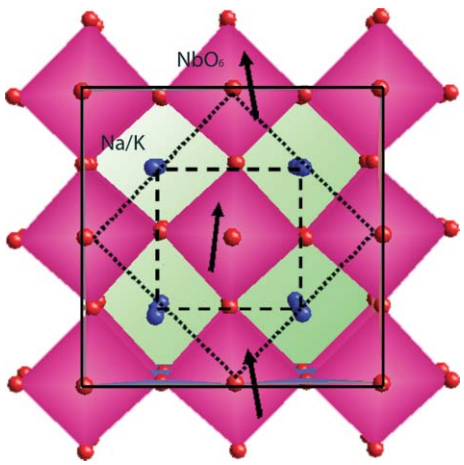

Fig. 1 Schematic of crystal structure of perovksite NKN comparing the monoclinic (*P*1*m*1, solid line, eight formula units per cell), orthorhombic (*Amm*2, dotted line, two formula units per cell) and the pseudocubic unit cell ($Pm\bar{3}m$, dashed line, one formula unit per cell). The arrows indicate octahedra tilting directions.

At the MPB composition, NKN has a very high dielectric constant[12] and good piezoelectric performance.[13] The good piezoelectric performance of NKN at the MPB composition is a two-tiered effect: (1) the off-centered Nb atoms displacement

[a]*Institute of Materials Research and Engineering, 3 Research Link, Singapore, 117602, Singapore. E-mail: g-goh@imre.a-star.edu.sg; Fax: +65 6874 4657; Tel: +65 6874 8346*
[b]*School of Materials Science and Engineering, Nanyang Technological University, Singapore, 639798, Singapore*

† Electronic supplementary information (ESI) available: (1) Normalized powder yield of the as-synthesized NKN, (2) TOPAS® refinement codes for NKN in *Amm*2 and *P*1*m*1 spacegroup. Further details of the crystal structure investigations shown in Table 1 may be obtained from the Fachinformationszentrum Karlsruhe, CSD-380418 to 380432. For ESI and crystallographic data in CIF or other electronic format see DOI: 10.1039/b923840a

during the cubic–tetragonal–orthorhombic phase transition with decreasing temperature,[14] and (2) the tilting of NbO_6 octahedra when sodium atoms replace potassium atoms, resulting in a structure shown in Fig. 1. The piezoelectric performance is improved further by introducing elements like lithium and antimony, resulting in an increased Curie temperature and piezoelectric properties comparable to a soft (donor-doped) PZT.[15]

$(Na_xK_{1-x})NbO_3$ is presently synthesized by conventional solid-state processes from potassium and sodium carbonate precursors at temperatures beyond 800 °C.[13,16,17] The high temperatures required during the solid-state process are problematic because potassium oxide starts to volatilize at 900 °C,[18] leading to non-stoichiometry,[19] lowered density[20] and ultimately, a degradation in the performance.[21] The solid-state process also requires over 80 h of laborious and high energy steps[22] including pre-mixing, attrition ball milling, calcination, and sintering. In particular, the milling steps unavoidably introduce contaminants from the milling media that cannot be removed later.[23] In contrast to the solid-state process, hydrothermal synthesis lowers the processing temperature from 800–1000 °C to 200 °C, processing times from 80 to 24 h[24] and removes the need for grinding or milling since submicron and nanosized particles can be obtained directly. In addition, epitaxial films required for miniaturized sensors and actuators can also be grown when a suitable substrate is introduced.[25,26]

While both pure $KNbO_3$ (KN) and $NaNbO_3$ (NN) powders have been successfully synthesized hydrothermally at low temperatures,[27–30] it appears that the formation of the NKN solid solution *via* hydrothermal synthesis is not so straightforward. In an earlier attempt to synthesize the NKN solid solution hydrothermally, Sun and co-workers[24] found that there was a big jump in the sodium occupancy from 24% to 89%. The abrupt increase in the sodium fraction prevented the formation of an NKN solid solution with the desired composition near the MPB – crucial for achieving its best properties. This report shows that sodium can be incorporated gradually into the NKN solid solution and demonstrates for the first time that NKN solid solutions with compositions near the MPB are achievable, clearly demonstrating the efficacy of the hydrothermal method in simplifying the current solid-state process.

Experimental

Hydrothermal synthesis and characterisation

NKN powder was-synthesized by reacting 1 g of Nb_2O_5 (99.99%, Aldrich, St. Louis, MO) in 25 ml aqueous mixtures of KOH (>88%, J.T. Baker, Phillipsburg, NJ) and NaOH (>98%, GCE) at 200 °C for 24 h in a PTFE-lined stainless steel autoclave (Parr Co., Moline, IL). The raw Nb_2O_5 precursor was identified to be a mixture of 91% H-Nb_2O_5[31] and 9% T-Nb_2O_5.[32] In all cases, the total $[OH^-]$ was fixed at 6 M because it was found to be the optimum concentration for the reaction to complete in 24 h at 200 °C. The solid solution composition was varied by changing the value of R from 0 to 20% where

$$R = \frac{[NaOH]}{[NaOH] + [KOH]}$$

After the reaction was completed, the resulting powder and solution were centrifuged at 3500 rpm for 10 min. The resulting supernatant was separated and tested for soluble niobate species by gradually replacing the solvent with cold ethanol (~−21 °C) or concentrated sodium hydroxide solution (2 M). The solvent replacement forces intermediate phases to precipitate due to lowered solubilities in these solvents.[30,33] The remaining powder slurry was washed with deionized water (Millipore, MA, resistivity >18.2 MΩ cm) at room temperature 4–5 times until the pH value was neutral as indicated by litmus paper. The white powder slurry was then dried at 60 °C in air for one day, weighed and stored in a dry box prior to further analysis. To investigate the effects of post-growth annealing on the as-synthesized powder's phase stability, heat treatment was carried out in a platinum-lined alumina crucible at 800 °C for 2 h with a ramp rate of 10 °C min^{-1}.

Early stages of NKN phase formation were observed by shortening reaction periods to three hours or less. Six samples with selected R values of 10% and 13.3% were prepared to represent the conditions with and without the second NN phase. The powder slurry, recovered by centrifugation, was then dried at 60 °C in air for one day, weighed and stored in a dry box prior to further analysis.

Phase content was analyzed by a Philips Multi-purpose Diffractometer with cobalt radiation at 40 kV and 40 mA, 0.01° step size, 30–150 s per step, and 2θ range from 10–150°. Energy-dispersive X-ray spectroscopy (EDS) elemental analysis was done using an OXFORD EDS system attached to a JEOL-5600 thermionic emission scanning electron microscope (SEM) on uncoated powder. Point analysis mode was chosen to standardize probe width, and live time was preset to 100 s to obtain statistically meaningful data. Results were taken by averaging ten randomly selected point readings. The powder morphology was characterized using a JEOL-6700F field emission scanning electron microscope (FESEM).

Refinement strategies

XRD data analysis and compilation was carried out using the Bruker® TOPAS 3 platform running in the fundamental parameters mode with known instrument parameters. Rietveld structure refinements of the NKN phases were carefully done based on the series of works by Ahtee and Hewat,[34,35] by assuming a rigid octahedral framework previously established by Megaw.[36] In accordance to the NKN phase diagram constructed by Tennery and Hang,[8] an orthorhombic *Amm*2 (No. 38, two formula units per unit cell) space group was used until the MPB was detected, after which the space group was replaced by a monoclinic *P*1*m*1 (No. 6, 8 formula units per unit cell). The refinable parameters were progressively released from the most stable parameters (*e.g.*, cell parameters) to the least stable (*e.g.* occupancy). Once the refinement had converged, normally within 3–4 refinement cycles, the cell parameter results from each sample were tabulated.

Although the atomic displacements on crossing the MPB result in a reduction in symmetry from orthorhombic to monoclinic, a pseudocubic unit cell (see Fig. 1) can be used for simplicity and convenience of comparing cell parameters across the different phases, with only a slight deviation from the

ideal (cubic) structure. The refinement results were therefore converted to a pseudocubic unit cell to enable a one-to-one comparison across the MPB. The refinement quality was checked by comparing the refinement results with the EDS data. A secondary check of Vegard's law validity within one phase was done by plotting the NKN refined cell volume against sodium occupancy in the NKN phase ("x") and comparing it to the reference data.[35,37]

An unknown hexaniobate phase was observed to form before the final perovskite phase. As it was believed to affect the phase purity of the NKN phase, analyzing it became important. The hexaniobate unit cell is made up two 'super-octahedrons'; each of these 'super-octahedrons' is made up of six edge-sharing NbO_6 octahedra[27] and so are significantly larger than the perovskite unit cells. Due to limited structural information, an alternative refinement strategy using a combination of the Pawley intensity fitting method[38] and the LeBail intensity extraction function combination[39] (referred to as whole powder pattern decomposition – WPPD – method[40]) was used to analyze the unknown hexaniobate phases. A preliminary qualitative analysis was done by manually matching the reflections of the raw XRD data with thirteen variants of hexaniobate-related compounds,[27,30,33,41,42] and the closest was found to be the sodium hexaniobate, $Na_7HNb_6O_{19}{\cdot}14H_2O$.[42] The initial unit cell parameters and other information was then taken from a Na-hexaniobate reference and refinement was run by only releasing the cell parameter values. Since the WPPD method does not determine the weight fraction of the different phases present in the powders, a Rietveld structure refinement of the powder was done by inserting the refined cell parameters of the hexaniobate phase determined with the WPPD method but using the atomic parameters of the sodium hexaniobate ($Na_7HNb_6O_{19}{\cdot}14H_2O$). Other reference data used in this study were obtained from previous works on $KNbO_3$,[43] $NaNbO_3$,[44] NKN,[35] Nb_2O_5[31,32] using the subscribed ICSD Database.[45] The actual and maximum niobium species yield of all samples were compared to ensure all of the niobium species were precipitated. Details of the refinement codes, steps and the generated atomic positions are available in the supporting materials section.

Results and discussion

The hydrothermal synthesis completes within 24 h, indicated by the high (≥97 wt%) NKN powder yield and the negative results from both the cold ethanol and the sodium hydroxide tests. Phase identification by X-ray diffraction (Fig. 2, only selected samples are shown for clarity) shows the samples are made up entirely of perovskite phases and that the NKN reflections are shifted towards higher 2θ with increasing R values. (Detailed results for all R values are tabulated in Table 1). These movements are indicative of a lattice contraction and that the smaller sodium atoms are successfully incorporated inside the potassium niobate (KN) lattice. It is also observed that for R values above 11.7%, a secondary phase identified as $NaNbO_3$ (NN) appears. Examinations of the phase-pure NKN powders by SEM and TEM show that the powders were made

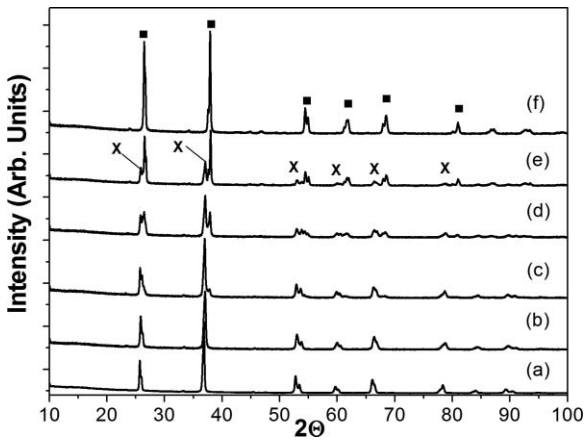

Fig. 2 X-ray diffraction of hydrothermally synthesized perovskite powders at 200 °C and 24 h for R values of (a) 0%, (b) 11.7%, (c) 13.3%, (d) 15%, (e) 18.3%, and (f) 100% showing the presence of NKN (crosses) and NN (filled squares).

Table 1 XRD data refinement results for all R values examined (estimated errors are shown in brackets)

		Lattice parameters				Sodium content (x)			
R (%)	NN 2nd phase (%)	a	b	c	NKN pseudo-cubic vol. (Å^3)	Occupancy refinement	EDS	From vol.	NKN phase[a]
0.0	0	4.0263(1)	3.9891(2)	4.0376(2)	64.849	0	0	0	M
1.7	0	4.0227(1)	3.9838(2)	4.0359(2)	64.677	0.07(1)	0.026	0.058	M
3.3	0	4.0215(1)	3.9820(1)	4.0357(1)	64.626	0.10(1)	0.038	0.076	M
5.0	0	4.0215(1)	3.9774(2)	4.0353(2)	64.545	0.10(1)	0.077	0.103	M
6.7	0	4.0167(1)	3.9746(2)	4.0320(1)	64.358	0.16(1)	0.104	0.149	M
8.3	0	4.0177(1)	3.9753(2)	4.0320(2)	64.396	0.17(1)	0.124	0.153	M
10.0	0	4.0165(1)	3.9726(1)	4.0331(1)	64.352	0.23(1)	0.161	0.168	M
11.7	0	4.0132(1)	3.9729(2)	4.0283(2)	64.228	0.24(1)	0.214	0.210	M
13.3	18.7	4.0134(1)	3.9706(2)	4.0295(2)	64.211	0.25(1)	[b]	0.216	M
14.2	47.4	4.0115(1)	3.9695(2)	4.0285(2)	64.149	0.28(1)	[b]	0.237	M
15.0	52.3	4.0101(1)	3.9701(1)	4.0267(2)	64.112	0.30(1)	[b]	0.250	M
15.8	70.6	4.0098(1)	3.9686(1)	4.0279(3)	64.056	[b]	[b]	0.269	M
16.7	67.4	4.0036(2)	3.9702(3)	4.021(1)	63.89	[b]	[b]	0.325	M
18.3	76.6	3.998(1)	3.961(1)	4.020(1)	63.636	[b]	[b]	0.411	M
20	93.1	3.94(1)	3.94(1)	4.036(3)	62.873	[b]	[b]	0.719	L

[a] Based on ref. 35. [b] Reliable data is unavailable due to the presence of the secondary NN phase.

up of single-crystalline cube-shaped particles, as confirmed by selected-area diffraction patterns of the particles. This is shown in Fig. 3 for powders obtained for an R value of 10%.

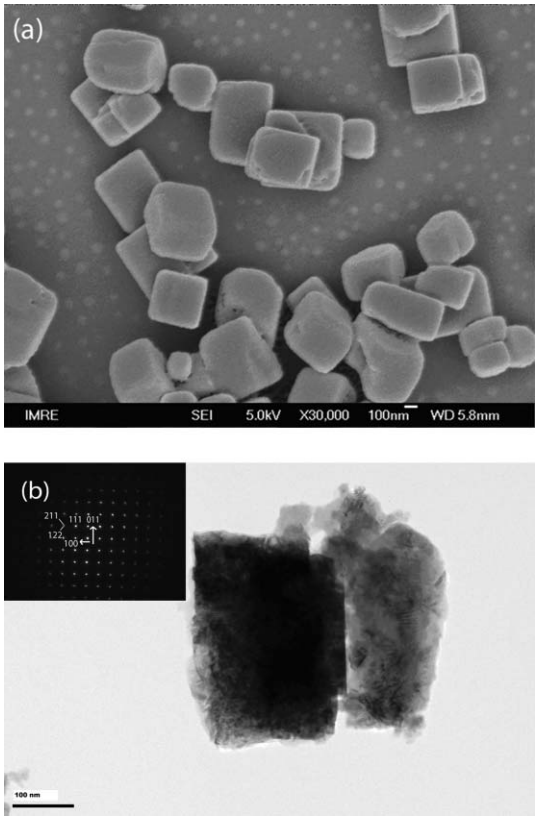

Fig. 3 Cube like morphology of as-synthesized NKN powder with R value of 10% as observed by (a) FESEM and (b) TEM (Inset: selected area electron diffraction of the left crystal along the [0$\bar{1}$1] axis, indicating an orthorhombic single-crystal phase).

Instead of analyzing the X-ray diffraction data using a peak indexing and visualization method (*e.g.* TREOR),[46,47] the Rietveld structure refinement method[48] is chosen for three reasons: (1) The Rietveld structure refinement is able to quantitatively analyze the X-ray diffraction data. The subtle movements of the X-ray diffraction data can be converted to accurate cell parameters, atomic positions, occupancies and thermal parameters. (2) Possibilities for ambiguity due to the presence of the second NN phase introduced by manual indexing are significantly reduced. (3) Increases in cell volume due to proton incorporation[27] in the NKN lattice complicates manual tracking of peak movements.

The Rietveld refinement is therefore applied to the entire as-synthesized NKN X-ray diffraction data, taking suitable structural information from the work by Ahtee and Hewat.[35] A good fit is obtained within 3–4 refinement cycles as indicated by the relatively small R-Bragg index value that ranges from 0.80 to 1.95. Fig. 4 is an example of such a refinement for a sample with an R value of 15%.

Rather than evaluating individual unit cell parameters, an assessment of the unit cell volume is more sensitive and appropriate in detecting the structural changes caused by an atomic substitution.[49] Therefore, the cell volume together with

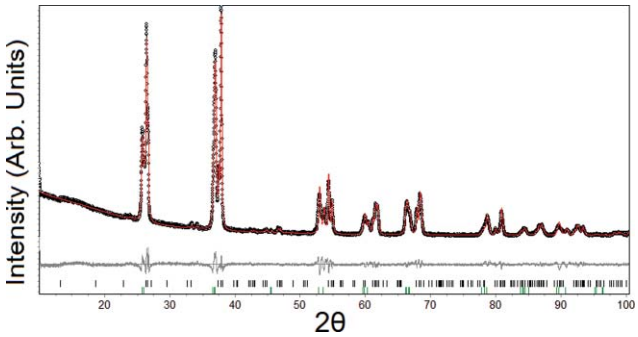

Fig. 4 Rietveld refinement of the X-ray diffraction profile of mixed NKN and NN powders precipitated at 200 °C showing experimental data (points), calculated (solid line), and the difference curve (bottom curve). Small vertical tick marks show reflection positions allowed by symmetry for each phase: NN (top) and NKN (bottom).

sodium occupancy as determined from cell volume, sodium occupancy as determined from diffracted intensities of the various cell reflections (occupancy refinement) and sodium occupancy according to EDS elemental analysis (only of single-phase samples) are plotted together in Fig. 5a. A gradual contraction of the NKN cell volume (left axis) followed by a corresponding increase of the sodium occupancy (right axis), x, in the NKN phase is observed from 0.03–0.3. Around an

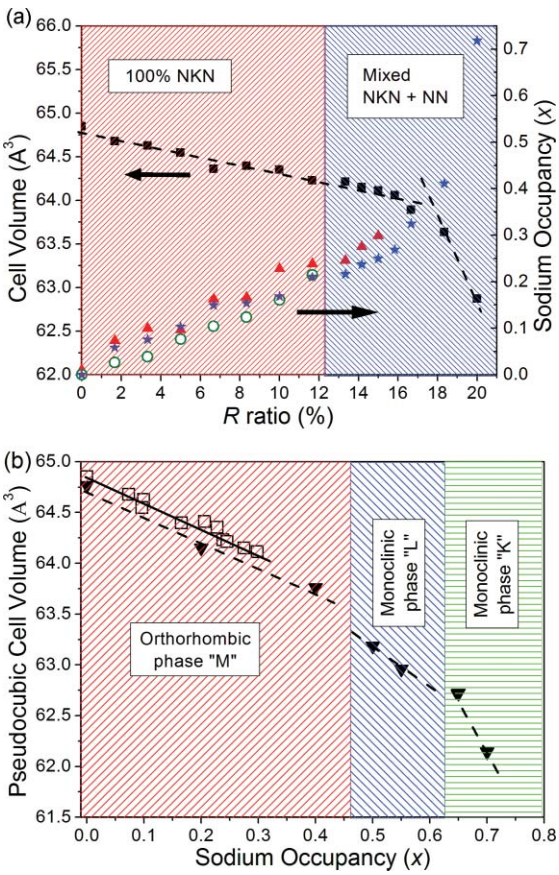

Fig. 5 (a) Plot of NKN cell volume (filled squares) against R and NKN sodium occupancy (x) obtained from occupancy refinement (triangles), EDS (open circles) and cell volume (stars) against R. (b) Plot of cell volume against sodium content of the as-synthesized single-phase NKN powder (open squares) and the reference data (inverted triangles).[37]

Table 2 NKN cell volume, sodium occupancy and phase composition after 2 h at 800 °C

	NKN cell volume (pseudo-cubic, Å^3)		x			NN 2nd phase (refined wt%)	
R (%)	Initial	After HT	Initial (from vol.)	After HT (from vol.)	After HT (EDS)	Initial	After HT
11.67	64.27	64.19	0.196	0.199	0.22	0	0
13.33	64.21	63.71	0.217	0.365	0.37	22.0(3)	0
13.75	64.19	63.45	0.222	0.491	0.45	26.7(2)	0
14.17	64.15	63.09	0.237	0.495	[a]	47.5(1)	10.2(1)
15.00	64.11	62.78	0.251	0.626	[a]	52.3(1)	12.7(1)
16.67	62.03	61.19	0.268	0.844	[a]	77.1(4)	26.3(1)

[a] Reliable data unavailable due to the presence of the secondary NN phase.

R value of 13.3%, the precipitated powder is no longer single-phase NKN but is a mixture of NKN and NN; with the sodium occupancy in the NKN phase still increasing. EDS analysis of the single-phase region agrees well with sodium occupancy values obtained from Rietveld refinement.

For NKN, the morphotropic phase boundary between the orthorhombic 'M' phase and the monoclinic 'L' phase occurs around an R value of 18.3% when a change in the rate of cell volume decrease (change in gradient in Fig. 5a) is detected. Unfortunately, the corresponding change in the rate of increase of sodium occupancy as determined from the occupancy refinement cannot be observed around the MPB because from an R value of 15.8%, around 70 wt% of the precipitated powder consists of sodium niobate. This makes it difficult to determine the sodium fraction in the minority NKN portion from the occupancy refinement since the diffracted intensities of the minor phase are overshadowed by the majority NN phase.

Alternatively, sodium occupancy can be determined from the cell volume, but only after it is determined that cell volumes vary with sodium occupancy according to Vegard's law. This is done by plotting the as-synthesized NKN cell volumes against the x values determined from the occupancy refinement, together with the reference data taken from Ahtee and Hewat.[37] As shown in Fig. 5b, two things are noticed. First, it is confirmed that the variation of cell volume with sodium occupancy for the NKN solid solution obeys Vegard's law.[50] Second, it is noticed that the cell volumes of the as-synthesized NKN powders are consistently ~0.1 Å^3 larger than the reference data. This lattice expansion has been observed previously for hydrothermally synthesized perovskite powders and is due to proton (hydroxyl ion and/or water) incorporation in the lattice.[51,52] It is important that this lattice expansion be taken into account during extraction of the sodium fraction from the respective cell volumes, since the lattice expansion would make it seem that lattice contraction on replacement of potassium with sodium is less. The sodium occupancy values extracted from the cell volumes is represented in Fig. 5a by filled star symbols and agree well with EDS and occupancy refinement values. More importantly, the change in the rate of increase in sodium occupancy also occurs in the region indicated earlier by cell volume data to be the MPB. In addition, it shows that NKN can by hydrothermally synthesized with compositions around the MPB.

So far, the hydrothermally synthesized NKN powders with compositions near the MPB ($x = 0.50$) are mixed with the NN phase. It is found that a short heat treatment at 800 °C for two hours is sufficient in converting the mixed-phase powders into single-phase NKN powders, as detailed in Table 2. Two important observations after the heat treatment are: (1) The NKN cell volume contracts significantly (>0.5 Å^3), accompanied by large increases (>50%) in sodium occupancy, x, in the $(Na_xK_{1-x})NbO_3$ powder. (2) The amount of secondary NN phase content is reduced after the heat treatment and for some R values, single-phase powders NKN powders are obtained. Most notably, a single-phase NKN powder with sodium occupancy, $x = 0.49$ near the MPB is obtained *i.e.* $(Na_{0.49}K_{0.51})NbO_3$. These findings indicate that an atomic exchange process between the potassium and sodium atoms is occurring – similar to what happens in the calcination step in the solid-state processing, except without significant weight loss (<0.5 wt%) because there are no carbonate precursors involved.

For the formation of NKN powders, most calcination processes usually require six or more hours in the temperature range 880–1000 °C in order to transform the mixed carbonate precursors into the desired perovskite solid solution.[13,16,17] The short conversion time in this study is attributed to two factors. Firstly, the two mentioned phases of NN and NKN are evenly distributed and in close proximity with each other, having been precipitated in the same solution. Secondly, the as-synthesized powder is already in the perovskite phase prior to heat treatment. Therefore, the total energy requirement will be lower because pure NKN phase can be formed by atomic exchange, requiring no precursor breakdown, carbonate removal or formation of a new crystal structure.

Intermediate hexaniobate phase

The appearance of a second sodium niobate (NN) phase during hydrothermal synthesis of NKN places some limits on the applicability of the hydrothermal method (*e.g.* a polymer nanocomposite cannot be made with NKN powders with compositions near the MPB). To understand the reason for the formation of the second phase, the early stages of NKN synthesis were studied by shortening the reaction period to three hours or less. Syntheses were chosen using R values of 10% and 13.3% as these represent the conditions that yield the pure NKN powder and mixed NKN and NN powders respectively.

As shown in Fig. 6, X-ray diffraction reveals that after 1 h, the precipitated powder consists of the starting Nb_2O_5 and a hexaniobate phase (only the diffractogram for the 10% sample is shown, as it is similar to the 13.3% sample). At 2 h, the

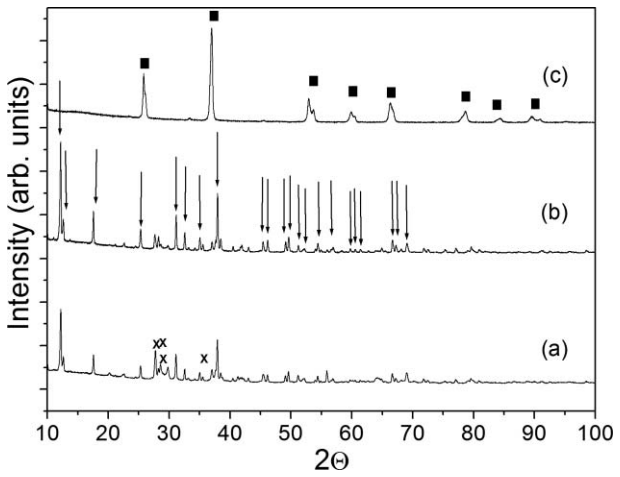

Fig. 6 X-ray diffraction spectra of powders after synthesis for (a) 1 h, (b) 2 h, and (c) 3 h for the 10% sample showing transformation of Nb_2O_5 (crosses) to NKN (filled squares) and the presence of an intermediate hexaniobate phase (arrows).

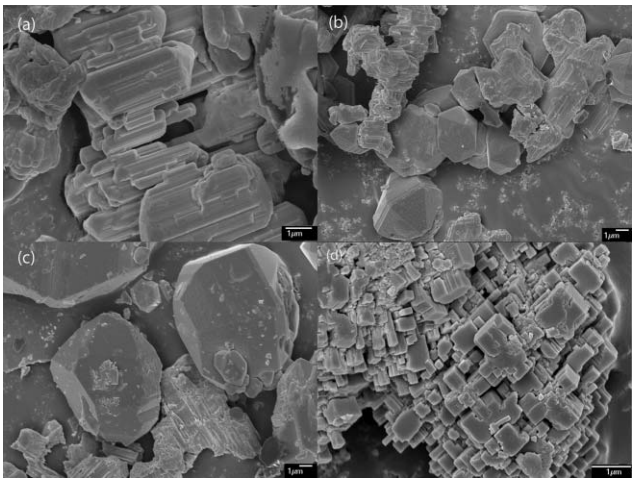

Fig. 7 Electron micrographs of (a) Nb_2O_5 precursor powder and powders obtained after (b) 1 h, (c) 2 h and (d) 3 h of synthesis for samples with $R = 10\%$.

same two phases are still present but for the R value of 13.3%, the NN phase is also present in the powder. Finally at 3 h, only the perovskite phases are present *i.e.* NKN for the 10% sample and NKN and NN for the 13.3% sample. A manual search-and-match identified the hexaniobate phase as sodium hexaniobate, $Na_7HNb_6O_{19}\cdot 14H_2O$.[42] It has been observed in the hydrothermal synthesis of KN that an intermediate hexaniobate phase can precipitate when the solution was left for long periods of time[27,53] or mixed with cold ethanol[30] before the formation of the perovskite phase occurred. In the case of NN, the precipitation of intermediate phase occurs more readily[33] and therefore different types of intermediate phases have been studied and reported.[29,30,54]

Corresponding scanning electron microscopy of the 10% sample showed that powder morphologies varied in line with changes previously revealed by XRD. As shown in Fig. 7b and c, from 1 to 2 h, Nb_2O_5 powder particles give way to large dodecahedra-shaped hexaniobate particles. Finally, as indicated by XRD, the familiar cube-shaped particles of the perovskite phase are attained at 3 h (Fig. 7d). It is not surprising to find large hexaniobate particles being replaced by sub-micron perovskite particles since a dissolution–reprecipitation process is required to form the perovskite phase. This is because the intermediate hexaniobate is composed largely of edge-sharing NbO_6 octahedra[27] (the lack of corner-sharing NbO_6 octahedra in the intermediate phase was also shown with the absence of light absorption near 300 nm, as described by Zhu *et al.*[54]) while the perovskite phase is composed of a 3D network of corner-sharing NbO_6 octahedra.

The Whole Powder Pattern Decomposition (WPPD) refinement method is then applied to the X-ray diffraction data to get the unit cell information. The space-group and unit cell information of the $Na_7HNb_6O_{19}\cdot 14H_2O$ obtained from the manual search and match method is taken as a starting point to represent the intermediate hexaniobate phase in the WPPD refinement. Other known phases such as NKN and Nb_2O_5 are also inserted in the refinement to calculate their weight percentage in the powder. The WPPD refinements that are run using only one type of hexaniobate phase quickly converged with R-Bragg values below one, an indication of a very good fit. Any attempts to include more than one phase of hexaniobate in one powder diffraction data leads to convergence failure or *hkl* phase redundancy. This is a strong indication that there is only one hexaniobate phase in each sample. The results of phase composition information and cell volume data obtained from the WPPD method are tabulated in Table 3.

It is noticed that the cell volumes of the hexaniobate phases for both the 10 and 13.3% samples (~1560 Å^3 and ~1565 Å^3 respectively) fall inbetween known cell volumes of sodium (1556.60 Å^3)[42] and potassium hexaniobate

Table 3 WPPD refinement data of 10% and 13.3% samples

	$R = 10.00\%$						$R = 13.33\%$					
			Phase composition (wt%)						Phase composition (wt%)			
Time (h)	Hexa cell volume (Å^3)	Na from EDS (%)	Hexa	Nb_2O_5	NN	NKN	Hexa cell volume (Å^3)	Na from EDS (%)	Hexa	Nb_2O_5	NN	NKN
1	1563.29(4)	0.321	45(1)	55(1)	0	0	1566.7(1)	0.455	93.0(2)	4.6(2)	0	2.5(1)
2	1559.72(4)	0.344	90.6(2)	9.4(2)	0	0	1566.4(1)	NA	79.7(4)	1.96(18)	15.4(3)	3.0(1)
3	NA	NA	0	0	0	100	NA	NA	0	0	13.3(1)	86.7(1)
24	NA	NA	0	0	0	100	NA	NA	0	0	18.7(2)	81.3(2)

The sum may not add up to 100% due to rounding.

(1583.75 Å^3).[55] This indicates that the intermediate hexaniobate phase formed was not $Na_7HNb_6O_{19}\cdot 14H_2O$ but a mixed hexaniobate, ($Na_yK_{(8-y)}Nb_6O_{19}\cdot nH_2O$). Energy-dispersive X-ray spectroscopy (EDS) carried out on samples without significant amounts of NN and/or NKN indicated that the 13.3% hexaniobate had 46% sodium while the 10% hexaniobate had 34%. It is believed that the mixed hexaniobate from the 13.3% sample had a larger cell volume than the 10% sample because of greater proton incorporation in the lattice, whether in the form of hydroxyl groups or water molecules. Lattice expansion due to proton incorporation was previously observed for hydrothermally synthesized group I:V perovskite powders by Goh and co-workers.[25,52]

Turning our attention back to Table 3, it is observed that only after the first hour, the phase compositions of the 2 samples are significantly different. For the 13.3% sample, less than 5 wt% of the Nb_2O_5 precursor is still present compared to >50 wt% for the 10% sample. This indicates that the Nb_2O_5 precursor is dissolved at a much faster rate for the 13.3% sample, much faster than what had been reported previously using only KOH solution with similar concentration.[56] Consequently, the intermediate hexaniobate ions for the 13.3% sample are formed more rapidly than for the 10% sample and the system is quickly pushed to supersaturation; evident in the very high amount of hexaniobate powder that precipitated for the 13.3% sample (>90 wt%). In order to relieve the supersaturation, the more stable perovskite phases are formed. In the case of the 10% sample, only the NKN perovskite phase is formed. In the case of the 13.3% sample, both NN and NKN phases formed and it is believed that precipitation of the NN phase helps to relieve the supersaturation of the system faster. Also, it is NN and not KN that forms as the second phase as NN is reported to form faster than KN.[27]

The large amount of the hexaniobate ions precipitated in concentrated KOH solution (an *R* value of 13.3% contains >5M KOH) at 200 °C however, was not expected, because the hexaniobates are known to be soluble in these conditions.[27,56] On the other hand, sodium hexaniobate is much less soluble.[27,33] Although sodium and potassium have the same ionic charge, sodium is slightly more electronegative and has a smaller ionic radius than potassium. This means a sodium-bonded atom pair will be shorter (*i.e.* stronger) and less polar compared to a potassium-bonded atom pair. As a result, a lot of sodium salts, including sodium hexaniobate,[33] are less soluble than the potassium salt. Therefore, it can be said that although sodium ions increase the solubility of the precursor Nb_2O_5 powder (note that the total OH concentration is the same for all samples), they decrease the solubility of the hexaniobate ion. More detailed understanding of how sodium affects the solubilities of these species appears to be the key to synthesizing single-phase NKN powders spanning the MPB.

Conclusions

In this study, sodium potassium niobate (NKN) solid solutions have been hydrothermally synthesized at 200 °C using simple KOH and NaOH mixtures with Nb_2O_5 precursor powders. Single-phase as-synthesized NKN powders with compositions up to $(Na_{0.24}K_{0.76})NbO_3$ were attained. When the concentration of NaOH compared to the total hydroxyl ion concentration, the *R* value, was above 11.7%, a second sodium niobate (NN) phase always formed along with the NKN phase. It was observed that sodium was gradually incorporated into the NKN phase with increasing *R* values, and a morphotropic phase boundary (MPB) between the orthorhombic–monoclinic NKN phases was found around an *R* value of 18%. Early stages of NKN formation revealed the presence of an intermediate mixed hexaniobate. It was observed that increasing *R* values were accompanied by the formation of a second NN phase as dissolution of the precursor Nb_2O_5 was speeded up, generating much greater supersaturation that was relieved by the formation of the NN phase.

It was also found that a short two hour heat treatment at 800 °C was effective in transforming the hydrothermally synthesized powders to a series of pure NKN powders with compositions up to $(Na_{0.49}K_{0.51})NbO_3$ – practically at the MPB. The short conversion time was attributed to intimate powder distribution and the fact that the hydrothermally synthesized powders were already in the perovskite phase. These findings suggest that hydrothermal synthesis can be applied as a step for making reactive precursors for use in a conventional solid-state process, simplifying the process flow and conserving the energy requirement. The improvements are achieved by removing the need to use hygroscopic carbonate precursors, and laborious and energy-intensive steps; such as attrition ball mixing, calcination and subsequent milling that are required to achieve desired composition prior to the final sintering step.

Acknowledgements

The authors thank Prof. T. J. White and Dr. Martin K. Schreyer for invaluable discussions and advice on crystal chemistry, refinement and parameter determination. The authors also thank Ms. Hui Hui Kim for conducting the TEM experiment.

Notes and references

1 V. M. Goldschmidt, *Trans. Faraday Soc.*, 1929, **25**, 253–283.
2 B. Jaffe, R. S. Roth and S. Marzullo, *J. Appl. Phys.*, 1954, **25**, 809–810.
3 R. E. Cohen, *Nature*, 1992, **358**, 136–138.
4 H. Needleman, *Annu. Rev. Med.*, 2004, **55**, 209–222.
5 A. Olaf, *J. Am. Ceram. Soc.*, 1919, **2**, 784–789.
6 M. Wicks, UK Ministry of Trade and Industry, The Stationery Office Limited, 2006.
7 G. Shirane, R. Newnham and R. Pepinsky, *Phys. Rev.*, 1954, **96**, 581–588.
8 V. J. Tennery and K. W. Hang, *J. Appl. Phys.*, 1968, **39**, 4749–4753.
9 U. Rick, *J. Am. Ceram. Soc.*, 2007, **90**, 3326–3330.
10 R. Guo, L. E. Cross, S. E. Park, B. Noheda, D. E. Cox and G. Shirane, *Phys. Rev. Lett.*, 2000, **84**, 5423.
11 H. Fu and R. E. Cohen, *Nature*, 2000, **403**, 281–283.
12 V. Lingwal and N. S. Panwar, *Ferroelectrics*, 2004, **300**, 3–14.
13 R. Zuo, J. Rödel, R. Chen and L. Li, *J. Am. Ceram. Soc.*, 2006, **89**, 2010–2015.
14 A. W. Hewat, *J. Phys. C: Solid State Phys.*, 1973, **6**, 1074–1084.
15 Y. Saito, H. Takao, T. Tani, T. Nonoyama, K. Takatori, T. Homma, T. Nagaya and M. Nakamura, *Nature*, 2004, **432**, 84–87.
16 M. Ichiki, L. Zhang, M. Tanaka and R. Maeda, *J. Eur. Ceram. Soc.*, 2004, **24**, 1693–1697.
17 D. Lin, K. W. Kwok and H. L. W. Chan, *J. Alloys Compd.*, 2008, **461**, 273–278.
18 U. Flückiger and H. Arend, *J. Cryst. Growth*, 1978, **43**, 406–416.
19 H. Kimura, A. Miyazaki, K. Maiwa, Z. X. Cheng and C. V. Kannan, *Opt. Mater.*, 2007, **30**, 198–200.

20 M. Matsubara, T. Yamaguchi, W. Sakamoto, K. Kikuta, T. Yogo and S.-i. Hirano, *J. Am. Ceram. Soc.*, 2005, **88**, 1190–1196.
21 V. Lingwal, B. S. Semwal and N. S. Panwar, *Ferroelectrics*, 2006, **332**, 219–225.
22 H. Nagata, K. Matsumoto, T. Hirosue, Y. Hiruma and T. Takenaka, *Jpn. J. Appl. Phys.*, 2007, **46**, 7084–7088.
23 J. De, A. M. Umarji and K. Chattopadhyay, *Mater. Sci. Eng., A*, 2007, **449–451**, 1062–1066.
24 C. Sun, X. Xing, J. Chen, J. Deng, L. Li, R. Yu, L. Qiao and G. Liu, *Eur. J. Inorg. Chem.*, 2007, **2007**, 1884–1888.
25 G. K. L. Goh, K. Y. S. Chan, B. S. K. Tan, Y. W. Zhang, J. H. Kim and T. Osipowicz, *J. Electrochem. Soc.*, 2008, **155**, D52–D56.
26 G. K. L. Goh, C. G. Levi, J. Hwan Choi and F. F. Lange, *J. Cryst. Growth*, 2006, **286**, 457–464.
27 G. K. L. Goh, F. F. Lange, S. M. Haile and C. G. Levi, *J. Mater. Res.*, 2003, **18**, 338–345.
28 A. J. Paula, R. Parra, M. A. Zaghete and J. A. Varela, *Mater. Lett.*, 2008, **62**, 2581–2584.
29 D. R. Modeshia, R. J. Darton, S. E. Ashbrook and R. I. Walton, *Chem. Commun.*, 2009, **7**, 68–70.
30 I. C. M. S. Santos, L. H. Loureiro, M. F. P. Silva and A. M. V. Cavaleiro, *Polyhedron*, 2002, **21**, 2009–2015.
31 K. Kato, *Acta Crystallogr., Sect. B: Struct. Crystallogr. Cryst. Chem.*, 1976, **32**, 764–767.
32 K. Kato and S. Tamura, *Acta Crystallogr., Sect. B: Struct. Crystallogr. Cryst. Chem.*, 1975, **31**, 673–677.
33 J. H. Kennedy, *J. Inorg. Nucl. Chem.*, 1961, **1961**, 53–57.
34 M. Ahtee and A. W. Hewat, *Acta Crystallogr., Sect. A: Cryst. Phys., Diffr., Theor. Gen. Crystallogr.*, 1975, **31**, 846–850.
35 M. Ahtee and A. W. Hewat, *Acta Crystallogr., Sect. A: Cryst. Phys., Diffr., Theor. Gen. Crystallogr.*, 1978, **34**, 309–317.
36 H. Megaw, *Acta Crystallogr.*, 1954, **7**, 187–194.
37 M. Ahtee and A. M. Glazer, *Acta Crystallogr., Sect. A: Cryst. Phys., Diffr., Theor. Gen. Crystallogr.*, 1976, **32**, 434–446.
38 G. Pawley, *J. Appl. Crystallogr.*, 1981, **14**, 357–361.
39 A. LeBail, H. Duroy and J. L. Fourquet, *Mater. Res. Bull.*, 1988, **23**, 447–452.
40 H. Toraya, *The Rigaku Journal*, 1989, **6**, 28–34.
41 C. H. Lin, C. H. Lee, J. H. Chao, Y. M. Huang, H. W. Chang, C. Y. Kuo and C. W. Hsu, *Mater. Chem. Phys.*, 2005, **92**, 128–133.
42 A. Goiffon, E. Philippot and M. Maurin, *Rev. Chim. Miner.*, 1980, **17**, 466–476.
43 V. A. Shuvaeva and M. Y. Antipin, *Cryst. Rep.*, 1995, **40**, 466–471.
44 A. C. Sakowski-Cowley, K. Lukaszewicz and H. D. Megaw, *Acta Crystallogr., Sect. B: Struct. Crystallogr. Cryst. Chem.*, 1969, **25**, 851–865.
45 P. Hewat, Fachinformationszentrum Karlsruhe and National Institute of Standards and Technology, 2007, http://icsdweb.fiz-karlsruhe.de.
46 B. Toby, *J. Appl. Crystallogr.*, 2005, **38**, 1040–1041.
47 P. E. Werner, L. Eriksson and M. Westdahl, *J. Appl. Crystallogr.*, 1985, **18**, 367–370.
48 H. Rietveld, *J. Appl. Crystallogr.*, 1969, **2**, 65–71.
49 C. J. Howard, E. H. Kisi, R. B. Roberts and R. J. Hill, *J. Am. Ceram. Soc.*, 1990, **73**, 2828–2833.
50 A. R. Denton and N. W. Ashcroft, *Phys. Rev. A: At., Mol., Opt. Phys.*, 1991, **43**, 3161.
51 S. Wada, T. Suzuki and T. Noma, *Jpn. J. Appl. Phys.*, 1995, **34**, 5368–5379.
52 G. K. L. Goh, S. M. Haile, C. G. Levi and F. F. Lange, *J. Mater. Res.*, 2002, **17**, 3168–3176.
53 S. Uchida, Y. Inoue, Y. Fujishiro and T. Sato, *J. Mater. Sci.*, 1998, **33**, 5125–5129.
54 H. Zhu, Z. Zheng, X. Gao, Y. Huang, Z. Yan, J. Zou, H. Yin, Q. Zou, S. H. Kable, J. Zhao, Y. Xi, W. N. Martens and R. L. Frost, *J. Am. Chem. Soc.*, 2006, **128**, 2373–2384.
55 M. Gasperin and M. T. Le Bihan, *J. Solid State Chem.*, 1982, **43**, 346–353.
56 H.-M. Zhou, D.-Q. Yi, Y. Zhang and S.-L. Zheng, *Hydrometallurgy*, 2005, **80**, 126–131.